

Numerical metric extraction in AdS/CFT

John Hammersley*

*Department of Mathematical Sciences,
Durham University, South Road, Durham DH1 3LE UK*

Abstract

An iterative method for recovering the bulk information in asymptotically AdS spacetimes is presented. We consider zero energy spacelike geodesics and their relation to the entanglement entropy in three dimensions to determine the metric in certain symmetric cases. A number of comparisons are made with an alternative extraction method presented in arXiv:hep-th/0609202, and the two methods are then combined to allow metric recovery in the most general type of static, spherically symmetric setups. We conclude by extracting the mass and density profiles for a toy model example of a gas of radiation in (2+1)-dimensional AdS.

1 Introduction

One of the original applications of the holographic principle was in relating the entropy of a black hole to the area of its horizon [1, 2]; since then a variety of authors have continued to explore relationships between bulk and boundary physics via holography, most notably via the AdS/CFT correspondence of Maldacena [3]. The idea of entropy being linked with an area rather than a volume (as one naturally expects from thermodynamics) is not, however, restricted to the case of black holes.

Recently, a proposal was put forward by Ryu and Takayanagi [4, 5] relating the entanglement entropy of a subsystem in a CFT to the area of a minimal surface in the bulk. This has been investigated further in a number of subsequent papers, such as [6, 7, 8, 9] where a number of related issues are explored. One avenue of interest leading from this proposal is the question of whether we can take this link between the entanglement entropy and minimal surface area, and devise a method to efficiently extract the bulk physics from the field theory information.

In (2+1) dimensions, the area of the minimal surface in question corresponds to the length of a static spacelike geodesic connecting the two endpoints of the region A through the bulk, as illustrated in figure 2. It is this observation that leads to

*J.C.Hammersley@dur.ac.uk

comparisons with a method of extracting the bulk metric given in [10], where the relation between singularities in correlation functions in the CFT and null geodesics (see [11] for details) was used to iteratively recover the bulk metric in certain asymptotically AdS spacetimes. In this paper we devise a similar method for extracting the bulk metric, using instead the relationship of Ryu and Takayanagi between the entanglement entropy and the length of the relevant spacelike geodesic. Interestingly, we find that after plotting the proper length against the angular separation of the endpoints, see figure 3, the gradient $d\mathcal{L}/d\phi$ immediately yields the angular momentum of the corresponding static spacelike geodesic. This simple relation then allows the minimum radius of the geodesic to be determined, and by working iteratively from large r , one can reconstruct the metric function of the bulk.

After describing the method and giving some examples of its application in practice, we then make a number of comparisons between this and the method of [10] (which is briefly reviewed in section 4.1). Most crucially, the two methods involve different ways of probing the bulk (as they involve different types of geodesic path), and whilst they appear computationally quite similar, this difference allows the method presented here to probe more fully a greater range of asymptotically AdS spacetimes. This is a consequence of the fact that in singular spacetimes, and those with a significant deviation from pure AdS, the effective potential for the null paths can become non-monotonic, resulting in geodesics which go into unstable orbits, see figure 12. This local maximum in the potential results in a finite range of radii which cannot be effectively probed by the null geodesics, and information about the bulk cannot be extracted; one does not encounter this problem when probing with static spacelike geodesics, provided the metric function is non-singular. Despite this advantage, one cannot use either method individually to extract information from the most general static, spherically symmetric spacetimes (those with a metric of the form of (26)), as neither can provide enough data with which to fully determine the metric; the null geodesics are not sensitive to the overall conformal factor of the metric, and the static spacelike geodesics cannot probe the timelike part. One can, however, use them in conjunction in order to do so. We thus conclude by proposing a combination of the two approaches such that the bulk information can be recovered, and give firstly an example demonstrating the ease with which it can be done, followed by a toy model setup of a gas of radiation (a “star”) in AdS_3 . We demonstrate how it is possible to determine both the star’s mass and density profiles from our estimates of the metric functions.

The outline of the paper is as follows: Section 2 contains background material on asymptotically AdS spacetimes and geodesic paths, and introduces the entanglement entropy relation from [4]. Section 3 develops the method for iteratively extracting the bulk metric, the full details of which are given in Appendix A, comments on the validity of the solutions, and goes on to give examples. In Section 4, after a review of the null geodesic approach from [10], the comparison between this and the spacelike method developed here follows, where we analyse their similarities and differences in applicability and efficiency. Finally, the two methods are combined in Section 5, to produce a more generally applicable method (as illustrated with the

recovery of the pertinent information about a “star” in AdS_3) and we go on to look at extensions of the method to less symmetric cases in section 6. We conclude in Section 7 with a discussion and summary of the results.

2 Background

Recall the metric for AdS_3 in coordinates (t, r, ϕ) :

$$ds^2 = -f(r)dt^2 + \frac{dr^2}{f(r)} + r^2d\phi^2 \quad (1)$$

$$f(r) = 1 + \frac{r^2}{R^2} \quad (2)$$

where R is the AdS radius. The existence of Killing vectors $\partial/\partial t$ and $\partial/\partial\phi$ leads to two conserved quantities (energy (E) and angular momentum (J)¹), and allows the geodesic equations to be written in the simple form:

$$\dot{r}^2 + V_{eff} = 0 \quad (3)$$

where $\dot{} = \frac{d}{d\lambda}$ for some affine parameter λ , and V_{eff} is an effective potential for the geodesics, defined by:

$$V_{eff} = - \left(f(r)\kappa + E^2 - \frac{f(r)J^2}{r^2} \right) \quad (4)$$

where $\kappa = +1, -1, 0$ for spacelike, timelike and null geodesics respectively. Note that only null and spacelike geodesics can reach the boundary at $r = \infty$ in finite coordinate time, and so these are the geodesics we work with when relating bulk physics to the boundary. The paths of a sample of null and spacelike geodesics through AdS_3 are shown in figure 1, where one observes that the null geodesics all terminate at the antipodal point on the boundary². This is in contrast to the spacelike geodesic endpoints, where there is a both an angular and temporal spread in their distribution, obtained by varying J and E (except in the $E = 0$ case, which we focus on here, where the geodesics are all contained in a constant time slice).

Consider a deformation³ to the pure AdS spacetime by replacing (2) with:

$$f(r) = 1 + \frac{r^2}{R^2} - p(r) \quad (5)$$

where $p(r)$ is an analytic function which is of comparable magnitude to r^2 at small r and tends to zero at large r . Now, in [10], the metric information was extracted by

¹Note that in [10], the geodesic angular momentum was denoted L ; here we use J to avoid confusion with L_T , which denotes the length of the system in the CFT (see section 3).

²This will not be the case in spacetimes which deviate from pure AdS_3 , see figure 11 in section 4.1.

³This is not the most general modification one could consider, however, in the more general case, one needs both null and spacelike probes to determine the metric, see section 5.

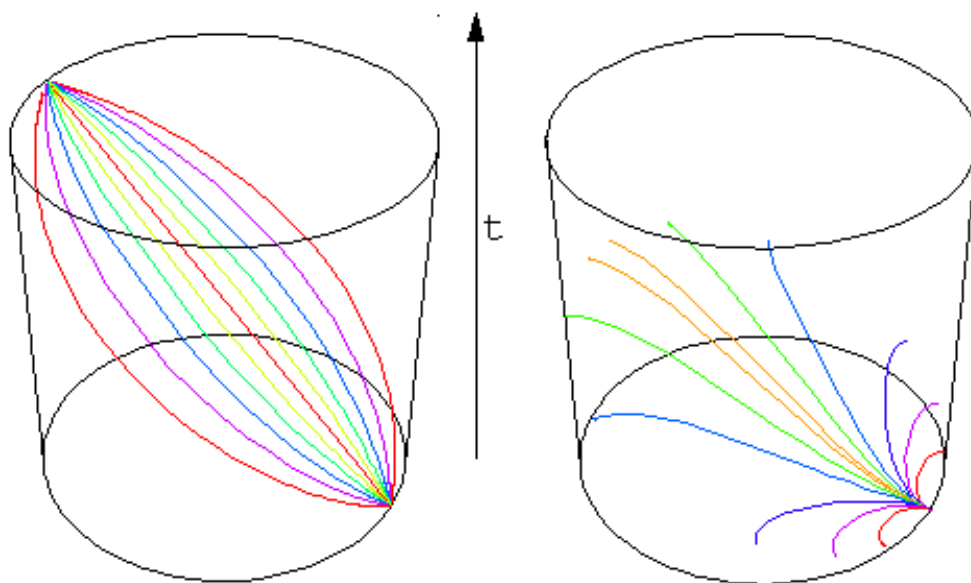


Fig. 1: A sample of geodesic paths in AdS_3 (with $R = 1$), all beginning at the same point on the boundary, with varying J and E . The null geodesics (left plot) all terminate at the same (antipodal) point, whereas this is not the case for spacelike geodesics (right plot).

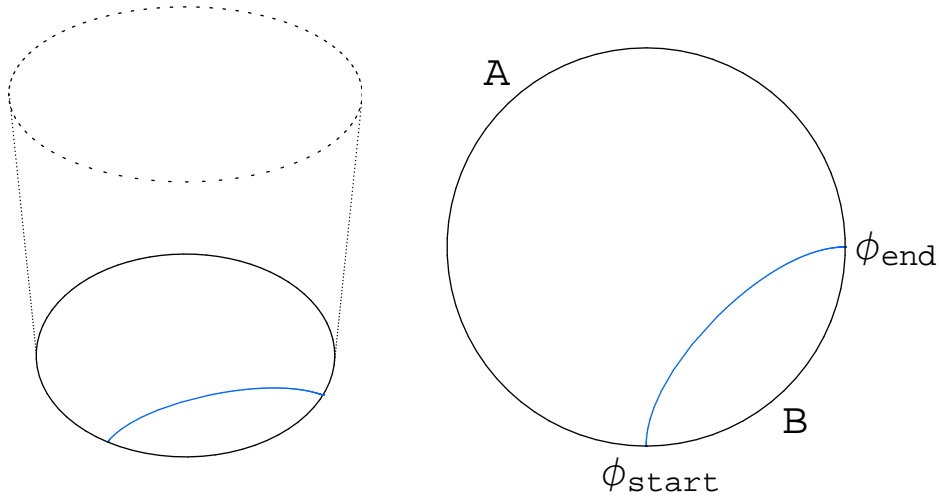


Fig. 2: A static spacelike geodesic in AdS_3 (left plot), with the regions A and B highlighted (right plot).

using the endpoints of null geodesics and their relation to correlation functions in the field theory. Here we propose to use the endpoints of static spacelike geodesics in three dimensions, and the relation between their proper length and the entanglement entropy of a two dimensional CFT proposed in [4] to extract the bulk information.

2.1 Entanglement entropy

In [4], Ryu and Takayanagi propose that the entanglement entropy S_A (in a CFT_{d+1}) of subsystem A with $(d - 1)$ -dimensional boundary ∂A is given by the area law:

$$S_A = \frac{\text{Area of } \gamma_A}{4 G_N^{(d+2)}} \quad (6)$$

where γ_A is the static minimal surface whose boundary is given by ∂A , and $G_N^{(d+2)}$ is the Newton constant in $(d + 2)$ dimensions. In the $d = 1$ case, γ_A will be given by a geodesic line, and thus if we consider AdS_3 with a (1+1)-dimensional CFT living on its boundary, and define two regions A and B on the boundary as in figure 2, Ryu and Takayanagi's proposal relates the proper length of the static spacelike geodesic shown to the entanglement entropy S_A . Thus by considering a complete set of these geodesics, we can probe the entire spacetime from out near the boundary down to the centre at $r = 0^4$, as we discuss in the following section.

⁴This assumes we are working in a non-singular spacetime; for the case where the central disturbance $p(r)$ corresponds to that for a black hole, one can probe down to the horizon radius, r_h , see section 4.3.

3 Method for reconstructing $f(r)$

Focussing on spacelike geodesics, and specifically those with zero energy (i.e. static), we have that:

$$\dot{r}^2 - f(r) \left(1 - \frac{J^2}{r^2}\right) = 0 \quad (7)$$

which can be combined with the angular momentum conservation equation $J = r^2 \dot{\phi}$ to give:

$$\frac{dr}{d\phi} = r \sqrt{f(r)} \sqrt{\frac{r^2}{J^2} - 1} \quad (8)$$

This can then be re-cast as an integral equation along the geodesic path, where we note that the final angular separation will be a function of J only:

$$\phi(J) \equiv \int_{\phi_{start}}^{\phi_{end}} d\phi = 2 \int_{r_{min}}^{r_{max}} \frac{1}{r \sqrt{f(r)} \sqrt{\frac{r^2}{J^2} - 1}} dr \quad (9)$$

where r_{min} is minimum radius obtained by the geodesic, and in the zero energy case is given simply by $r_{min} = J$. As the metric is divergent at the boundary $r = \infty$, we introduce a cut-off r_{max} and restrict ourselves to the region $r < r_{max}$.⁵ We also have that the proper length of the geodesic (also dependent only on J) is given by:

$$\mathcal{L}(J) = 2 \int_{r_{min}}^{r_{max}} \frac{1}{\sqrt{f(r)} \sqrt{1 - \frac{J^2}{r^2}}} dr \quad (10)$$

These two equations, (9) and (10), will form the basis for our method of extracting the metric function $f(r)$ at each r .

Now, given that the spacetime in which we are working is asymptotically AdS, we can say that for $r \geq r_n$ for some r_n which can be arbitrarily large (but still below the cut-off r_{max}), $f(r) \approx r^2 + 1$ (with R set to one). Thus all static spacelike geodesics with angular momentum $J \geq J_n \equiv r_n$ will remain sufficiently far from the central deformation $p(r)$ such that they remain undisturbed by its effects, and in the limiting case $J = r_n$ we can write:

$$\phi_n = 2 \int_{r_n}^{r_{max}} \frac{1}{r \sqrt{r^2 + 1} \sqrt{\frac{r^2}{r_n^2} - 1}} dr \quad (11)$$

$$= \frac{\pi}{2} - \arctan \left(\frac{2r_n^2 + (r_n^2 - 1) r_{max}^2}{2r_n \sqrt{r_{max}^4 - (r_n^2 - 1) r_{max}^2 - r_n^2}} \right) \quad (12)$$

$$\approx \frac{\pi}{2} - \arctan \left(\frac{r_n^2 - 1}{2r_n} \right) \quad \text{for } r_{max} \gg r_n \quad (13)$$

⁵This cut-off corresponds to the ratio between the UV cutoff (or equivalently the lattice spacing) in the CFT and the total length of the system: $r_{max} \sim L_T/a$

where $\phi_n = \phi_{end} - \phi_{start}$, and is the length of section B of the boundary in figure 2. Hence from the ϕ endpoints, which are specified by the our choice of region A in the CFT, we can determine r_n and we have that $f(r_n) = r_n^2 + 1$. This will be the starting point for an iterative method which will recover the metric from r_n down to zero (in the non-singular case).

The naive way in which to now proceed is by taking a slightly smaller choice of minimum radius, $r_{n-1} < r_n$, and splitting up the relevant integrals in (9) and (10) into two pieces, one from r_{n-1} to r_n and one from r_n to r_{max} . These integrals could then both be well approximated, the first by taking a series expansion about the minimum radius r_{n-1} , and the second by approximating the spacetime as pure AdS, as in (11). We would thus end up with two simultaneous equations which could be solved to give r_{n-1} and $f(r_{n-1})$, and could then proceed in a similar fashion to obtain the the entire bulk metric, to an arbitrary level of accuracy determined by our choice of step size in r (which is determined by our choice of boundary region $\phi_{end} - \phi_{start}$). However, it turns out there is a significant problem with this setup which prevents it being applied in practice. Specifically, the iterative process is unstable, with any errors in the estimates for r_{n-i} and $f(r_{n-i})$ leading to greater errors at the next step. This results in a rapid divergence of the estimate from the actual metric, and the iteration quickly breaks down. Whilst improving the approximations to the various terms in the integral can slightly improve matters, there is a way of avoiding this unstable setup (where we solve for the two unknowns simultaneously at each step) entirely, as we shall now demonstrate.

3.1 Determining the angular momentum

Consider the equations (9) and (10) above; they both have very similar forms, and there is in fact a strikingly simple yet powerful relation between the two quantities, \mathcal{L} and ϕ . Taking the derivative of both with respect to J , the angular momentum, we have that:

$$\frac{d\mathcal{L}}{dJ} = 2 \int_{r_{min}}^{r_{max}} \frac{J}{r^2 \sqrt{f(r)} \left(1 - \frac{J^2}{r^2}\right)^{3/2}} dr - \left(\frac{2}{\sqrt{f(r)} \sqrt{1 - \frac{J^2}{r^2}}} \right) \Big|_{r=r_{min}} \frac{dr_{min}}{dJ} \quad (14)$$

and

$$\frac{d\phi}{dJ} = 2 \int_{r_{min}}^{r_{max}} \frac{1}{r^2 \sqrt{f(r)} \left(1 - \frac{J^2}{r^2}\right)^{3/2}} dr - \left(\frac{2J}{r^2 \sqrt{f(r)} \sqrt{1 - \frac{J^2}{r^2}}} \right) \Big|_{r=r_{min}} \frac{dr_{min}}{dJ} \quad (15)$$

Using the fact that $J = r_{min}$, and noting that the divergent part of the integral cancels with the divergent second term in each equation⁶, we can see that the two equations are identical upto a factor of J , and we therefore have that:

⁶It is straightforward to show this, and an equivalent calculation is given explicitly in the second appendix of [10].

$$\frac{d\mathcal{L}}{dJ} = J \frac{d\phi}{dJ} \quad (16)$$

which can be rewritten as

$$\frac{d\mathcal{L}}{d\phi} = J = r_{min} \quad (17)$$

Thus we have the remarkable fact that the minimum radius⁷ of the static space-like connecting any two points on the boundary is immediately calculable from the gradient of a plot of the proper length, \mathcal{L} versus angular separation ϕ , see figure 3. This immediately provides us with one of the two unknowns we need at each step, and leaves us with only needing to calculate $f(r_{min})$. This can be done iteratively, beginning at large r , by splitting up (9) (or (10)) and taking various approximations to each part of the integral, the full details of which are given in Appendix A. Unlike the original proposal for the method, this is very robust to any errors, and provides an efficient way of determining the bulk structure, as we see in the examples in the following section.

The relation (17) also allows us to more specifically determine the point at which the metric deviates from pure AdS; recall that on the first step of the iteration (with $i = 0$), we took the metric to be pure AdS, and after determining r_n using (11), set $f(r_n) = r_n^2 + 1$, where we originally stated that r_n could be taken arbitrarily large. We can now explicitly check the radii at which the pure AdS assumption holds, as we can now determine the value of r_{min} corresponding to each ϕ separation of the endpoints, and hence plot r_{n-i} vs ϕ_{n-i} for each i . In pure AdS, we know that the relation is given analytically by $r_{min} = \cot(\frac{\phi_{end} - \phi_{start}}{2})$, and at small enough angular separation, the two plots should coincide (this is also of course true on the plot of \mathcal{L} vs ϕ , see figure 3). This allows one to avoid beginning the iteration at an excessively large radius, which would reduce the efficiency of the extraction.

We now address the issue of how confident one can be that the extracted solution matches the actual metric, before going on to consider some examples.

3.2 Validating the extracted solution

A natural question to ask at this point is on the uniqueness of the solution, i.e. is there more than one possible $f(r)$ which gives the same boundary data for the geodesics? Then if there is a unique $f(r)$, does this proposal for reconstructing the metric always find it, and not some alternative set of points $(r_{n-i}, f(r_{n-i}))$ which also solve equations (50) and (56) without being the actual metric function?

Considering the second question, it is quite simple to show that if the metric function $f(r)$ corresponding to the boundary data is unique, then the iterative method

⁷Note that equation (17) holds in any static, spherically symmetric spacetime; in those with less symmetry, such as angular variation of the metric as well as radial, one finds that the gradient $\frac{d\mathcal{L}}{dJ}$ gives the final angular momentum of the geodesic, but as this will not be conserved, it is not necessarily equal to r_{min} .

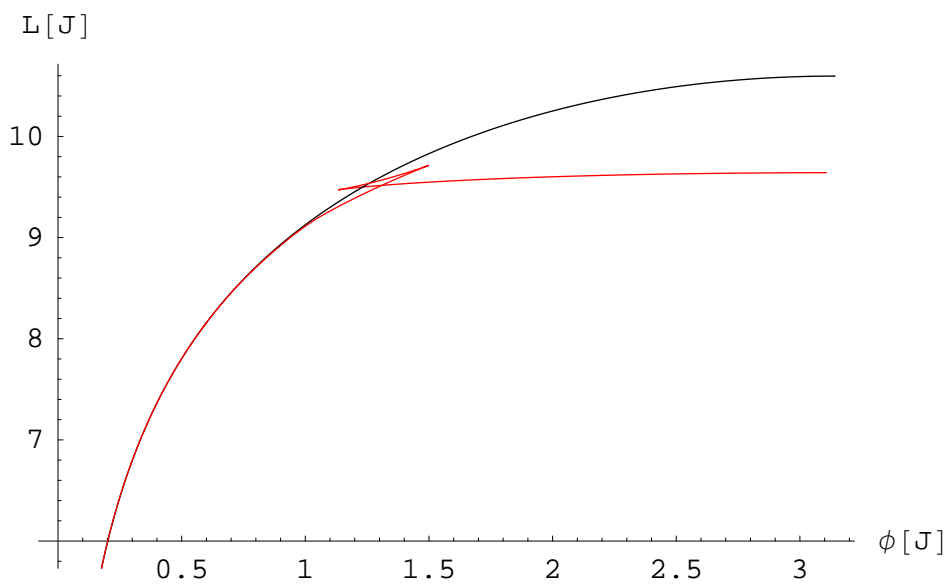


Fig. 3: A plot of the proper length, \mathcal{L} , vs the angular separation of the endpoints, ϕ , for static spacelike geodesics in an asymptotically AdS spacetime (red, lower curve), and in pure AdS (black, upper curve). The gradient, $d\mathcal{L}/d\phi$ at each point provides the angular momentum, J , for the corresponding geodesic. When the angular separation is small, the geodesics remain far from the centre, away from the deformation, and hence both curves coincide.

must recover it (up to a level of accuracy determined by the number of steps). We will show that if this is not the case, then either the metric function was not unique, contradicting our assumption, or the estimate does not in fact correspond properly to the boundary data.

Take the extracted points $(r_{n-i}, f(r_{n-i}))$ for $i = 0, \dots, n$, and use them to construct an interpolation function, which is then our estimate for the metric function. We can then use this estimate to compute the proper length and angular separation of all spacelike geodesics passing through the spacetime. If the generated data matches with the original data from the field theory, we have successfully produced an estimate for an actual bulk metric, and by our assumption of uniqueness, this function must be $f(r)$.

If the generated data fails to match correctly to that from the field theory, we can deduce that we haven't in fact produced an estimate for $f(r)$, but instead that our $(r_{n-i}, f(r_{n-i}))$ are simply a set of points which solve the equations (50) and (56). In this case, the iterative step size used to produce the estimate was too large, and the extraction procedure should be repeated with a smaller step size. Once the new estimate has been produced, the above test can again be applied; this can continue until an actual estimate of $f(r)$ is recovered.

Finally, one should note that at an infinitesimally small step size, one will use the complete⁸ set of spacelike geodesics to probe the spacetime, generating a continuous estimate for $f(r)$ from r_n down to zero. As such the data generated from our estimate must correspond to that from the field theory, as it was all used in its production. Thus, by uniqueness, the estimate must correspond to $f(r)$.

A basic argument for the uniqueness of the bulk metric corresponding to the field theory data (in our case, the proper length of the static spacelike geodesics as a function of the angular separation of the endpoints) follows from a comparison of the local degrees of freedom on each side, by noting that this data and the geometry of the constant time slice we wish to recreate contain the same amount of information, as $f(r)$ is a function of the radial coordinate only. When coupled with the knowledge asymptotic behaviour of the spacetime (that it approaches pure AdS at large r), we have the boundary conditions needed to ensure that the metric function is unique. In less symmetric cases one has more freedom in the metric, but correspondingly one also has more information with which to determine this, see section 6 for further comments on these scenarios.

Finally, one should note that this is simple argument does not constitute in any way a proof of the existence or uniqueness of the solution, as here the focus is on demonstrating how an intriguing link between field theory and the bulk leads to a remarkably simple process for calculating numerically the corresponding bulk metric. With this in mind, having argued that with suitable checks the extracted solution should be an estimate for $f(r)$, we now proceed to some examples where we examine the accuracy of such estimates.

⁸By complete, we mean all geodesics which have minimum radius $r_{min} \leq r_n$, where r_n can be taken arbitrarily large

Step size	α (4)	β (1)	γ (8)	χ (3)	η (2)	λ (1)
0.1	3.75	0.70	7.99	3.03	1.99	1.00
0.05	3.81	0.79	7.95	3.02	1.99	1.00
0.01	3.94	0.85	8.19	3.01	2.00	1.00
0.005	3.95	0.93	8.01	3.01	2.00	1.00

Table 1: Best fit values (to 2 d.p.) for the $f_{\text{fit1}}(r)$ parameters α , β , γ , χ , η and λ , with the actual values indicated in brackets.

3.3 Examples

To illustrate the procedure for metric extraction, we begin by considering some examples of deformations of the pure AdS metric. In the cases considered we have taken the proper length and angular separation of the endpoints to be known from the relevant field theory, and taken a linear step size in J (and hence r_{min}). The method of Appendix A is then applied for a variety of step sizes, and the resulting estimates for $f(r)$ are plotted alongside the actual curve. The three deviations from pure AdS we consider are the following:

$$f_1(r) = 1 + r^2 - \frac{4r^2}{(r^2 + 1)(r^2 + 8)} + \frac{3r \sin(2r)}{r^4 + 1} \quad (18)$$

$$f_2(r) = 1 + r^2 + \frac{10 \sin^2(3r)}{r^3 + 1} \quad (19)$$

$$f_3(r) = 1 + r^2 + \frac{10 \sin^2(10r)}{r^3 + 1} \quad (20)$$

where each gives a non-singular, asymptotically AdS spacetime. These functions were chosen as tests of the extraction method because they provide clearly visible deviation from the pure AdS metric of $f(r) = r^2 + 1$. The first example also corresponds to one used in [10] in an alternative method for extracting the bulk information (see section 4), and despite the similarities between $f_2(r)$ and $f_3(r)$, we shall see a noticeable difference in the accuracy of their extraction for larger step sizes.

For the first example we use four choices of step size in r , namely $\Delta r \approx 0.1, 0.05, 0.01$ and 0.005 , and compare the accuracy of the generated curves to the actual function; this is done by considering best fits to the numerical estimates, obtained by using a non-linear fit to the following function:

$$f_{\text{fit1}}(r) = 1 + r^2 - \frac{\alpha r^2}{(r^2 + \beta)(r^2 + \gamma)} + \frac{\chi r \sin(\eta r)}{r^4 + \lambda} \quad (21)$$

to give values for the various parameters. The results are shown in Table 1, with the corresponding data points plotted in figures 4 and 5.

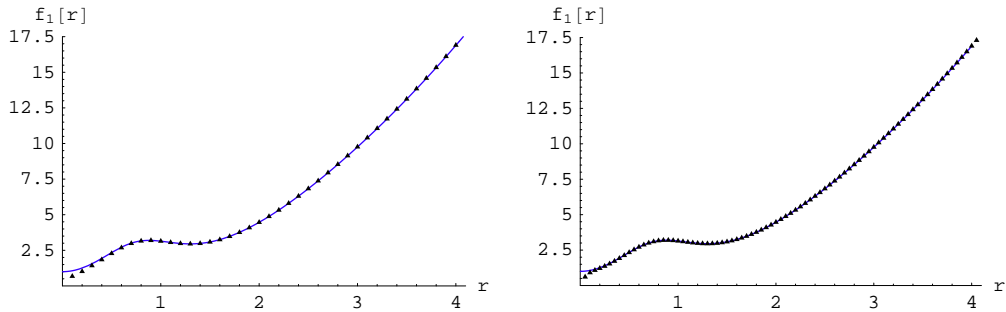


Fig. 4: The data points for the largest two step size estimates for $f_1(r)$, compared with the actual curve (in blue). Whilst both give good estimates to the curve, the step size of 0.1 (left) deviates at a higher r than when using a step size of 0.05 (right).

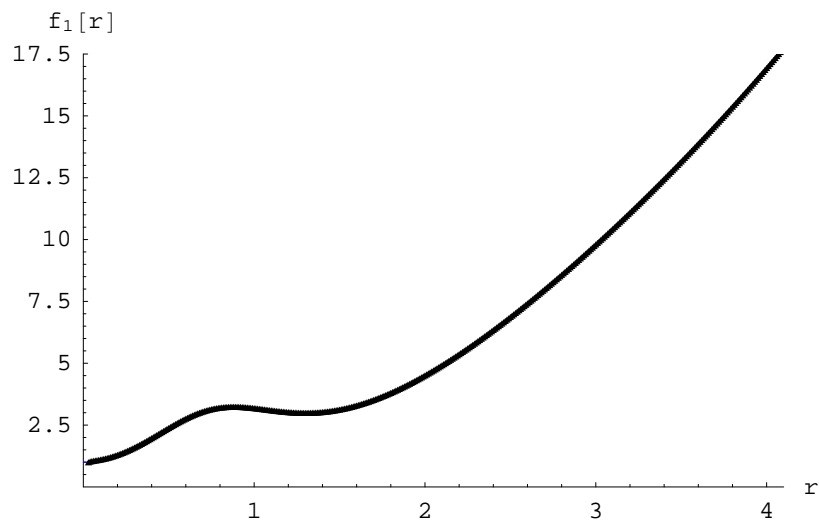


Fig. 5: The data points for the next-to-smallest step size estimate for $f_1(r)$, compared with the actual curve (in blue). The fit here appears very good even close to $r = 0$, however, Table 1 shows that we still need to go to a smaller step size in order to accurately extract values for α , β and γ .

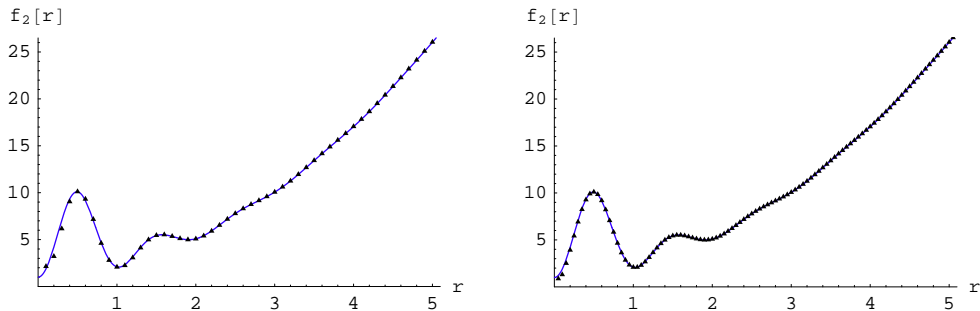


Fig. 6: The data points for the largest two step size estimates for $f_2(r)$, compared with the actual curve (in blue). Despite the larger deviation from pure AdS than in example 1, both the estimates here provide good fits to the curve.

Step size	χ (10)	η (3)	λ (1)
0.1	10.32	2.99	1.06
0.05	10.08	3.00	1.01
0.01	10.05	3.00	1.01

Table 2: Best fit values (to 2 d.p.) for the $f_{\text{fit}2}(r)$ parameters χ , η and λ , with the actual values indicated in brackets.

From Table 1, which contains the data for the estimates of $f_1(r)$ we see that there is a very good fit to the actual values of the six parameters from our non-linear fit (21), even at the largest step size we consider. Indeed, by eye it is hard to tell any difference between the accuracy of the estimates except at very small radii. This is mainly due to the relatively slow variation of $f_1(r)$ with r , which ensures the various approximations we take in order to produce the estimates remain good even for the larger step sizes. Whilst it appears that taking a smaller step size is rather superfluous, it should be noted that the finer structure parameters (namely α , β and γ) would need the smaller step size data in order to be determined to a high level of confidence. Our choice of non-linear fit function is also rather specifically chosen to match the example; if one did not know beforehand the form of $f_1(r)$ one would want to take smaller step size estimates in order to obtain data down as close to $r = 0$ as possible (as is discussed at the end of the section), to ensure that any finer structure was not being masked, and also as a check on the validity of the previous estimate.

We see similar behaviour in the second example, where we have chosen a slightly more fluctuating function to attempt to recover. Here we use the three largest choices of step size in r , and the data generated in each estimate is shown in figures 6 and 7, where we also include a plot of the actual function $f_2(r)$ as comparison.

We can again use a non-linear fit to evaluate the estimate; in this case we use a

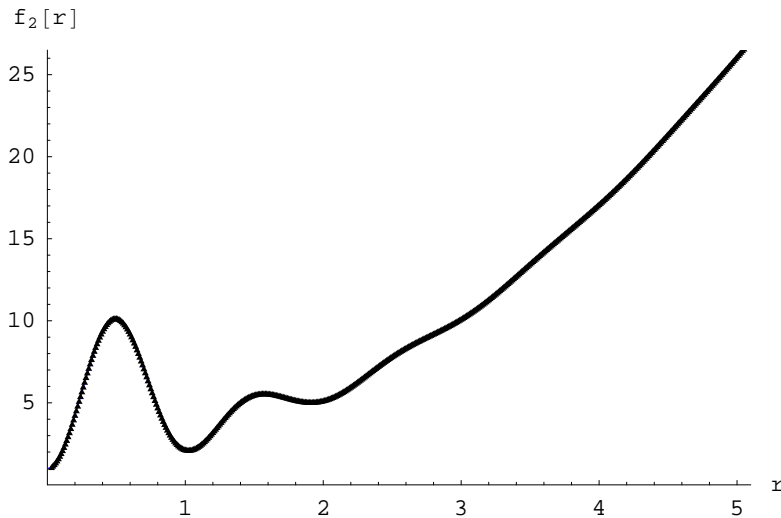


Fig. 7: At a step size of 0.01, the estimate data for $f_2(r)$ matches the actual curve (in blue) almost exactly, even close to $r = 0$.

Step size	χ (10)	η (10)	λ (1)
0.1	7.49	8.03	0.29
0.05	11.60	10.00	1.25
0.01	9.96	9.99	0.99

Table 3: Best fit values (to 2 d.p.) for the $f_{\text{fit}2}(r)$ parameters χ , η and λ , with the actual values indicated in brackets.

function of the form:

$$f_{\text{fit}2}(r) = 1 + r^2 + \frac{\chi \sin^2(\eta r)}{r^3 + \lambda} \quad (22)$$

and the results are shown in Table 2.

Thus far everything is progressing as expected: the smaller step sizes are producing closer fits to the curve, and better estimates for the values of the various parameters. In these first two examples, we even have that the largest step sizes produce good fits to the curves; do we ever see a large increase in accuracy over our choice of step size? If we consider the third example (which was obtained by increasing the value of η from the second example), where the function oscillates more wildly at low r , we do see a significant improvement in the estimates as the step size decreases. Proceeding as before, we see that for the largest step size of 0.1, the method has difficulty in following the rapid oscillations at low r ; this is then significantly improved upon in the subsequent estimates, as shown in figures 8 and 9, and in the non-linear fit data given in Table 3.

As expected, the smaller step size again produces a closer fit to the actual curve,

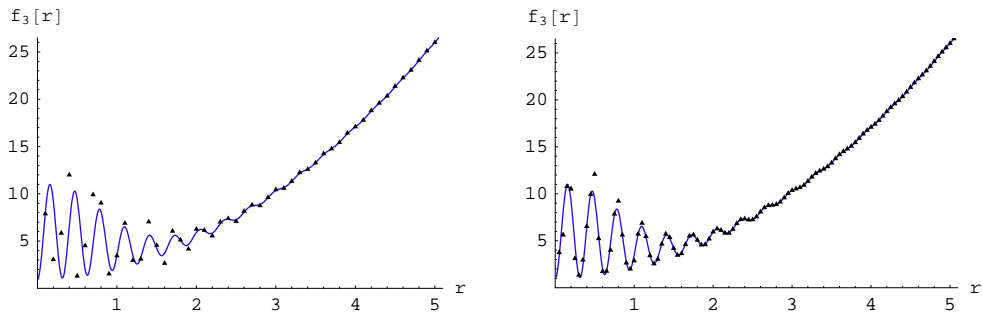


Fig. 8: The data points for the largest two step size estimates for $f_3(r)$, compared with the actual curve (in blue). The reduction in step size from 0.1 (left) to 0.05 (right) gives a marked improvement in the fit of the points to the curve at low r .

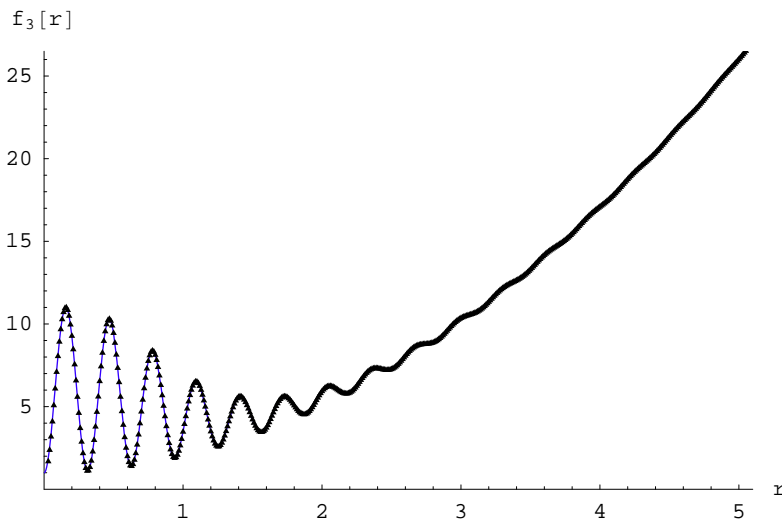


Fig. 9: The data points for the smallest step size estimate for $f_3(r)$, compared with the actual curve (in blue). This level of precision gives a very good fit to the curve, and this is mirrored in the highly accurate estimates for the function parameters, given in Table 3

however, in this third example, the largest step size fail to give accurate data for the unknowns χ , η and λ , although it does make a reasonably close fit to the curve until the iterative process breaks down.

Finally, one should comment on the fact that the deviation of the estimate from the actual curve does not apparently prevent the iteration from continuing to give sensible looking (although erroneous) values in subsequent steps. Whilst appearing to allow for an incorrect determination of the metric, applying the checks described in section 3.2 (reconstructing the field theory data using the metric estimate) will quickly highlight any areas in which the estimate for $f(r)$ has deviated from the correct function. As stated before, this merely indicates that the step size in r was too great for the iterative method to properly be effective in extracting the information using the approximations chosen in Appendix A. Aside from simply reducing the step size, or using better approximations (such as at each step creating an interpolating function estimate for $f(r)$ using the already determined data), there are other possible resolutions of this problem to further optimise the extraction. One could take either a non-linear step size in r to include more terms near $r = 0$, or simply take appropriately varying step sizes depending on the fluctuations of the metric; where the metric is varying rapidly with r the step size could be reduced. Thus by making several passes, reducing the step sizes at appropriate r each time, the estimate of $f(r)$ can be significantly improved without considerably increasing the computation time.

We now conclude the examples section by briefly investigating how the method is affected in spacetimes with a wildly fluctuating interior, and how one can apply the above to maintain a high degree of accuracy.

3.4 Maintaining accuracy in wildly fluctuating spacetimes

The third example of the previous section has shown that in wildly fluctuating spacetimes one needs smaller step sizes in order to guarantee accuracy of the estimate for $f(r)$ down to small r . Here we provide two further examples to show how the method breaks down if the frequency of the fluctuations is sufficiently increased, and how one can adjust the step size to compensate.

Firstly, one observes that it is not simply the frequency of the oscillation which causes the extraction to break down, but also the amplitude; this can be seen in figure 10, where the estimate continues to follow the actual curve closely whilst the amplitude of the oscillations is small. The two examples shown in the figure come from considering modifications to example 3 where the $\sin^2(10r)$ term is replaced by first $\sin^2(20r)$ and then $\sin^2(30r)$; as stated, one still obtains a relatively good fit to the curve using the smallest step size, although in the more rapidly oscillating case the fit does deviate slightly more from the correct curve, especially near the peaks at low r .

This behaviour is important, as it means that even in metrics with a large and rapidly varying interior, one can use a reasonable step size to extract the metric with confidence down to a fairly close distance to the centre. After checking the estimate

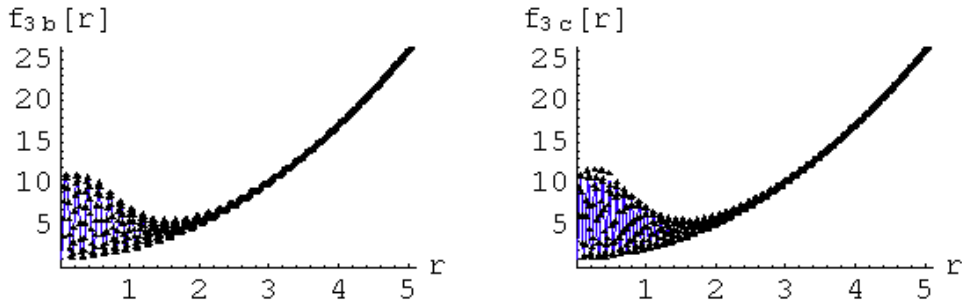


Fig. 10: Plots of $f_3(r)$ with the $\sin^2(10r)$ term replaced by $\sin^2(20r)$ (left) and $\sin^2(30r)$ (right), along with estimates generated with a step size of 0.01. Interestingly, whilst sufficiently increasing the frequency of the metric oscillations does reduce the depth to which the metric is accurately extracted, it does not adversely affect the accuracy of the fit to that point.

by recreating the field theory data, one can then continue the extraction from that point with better approximations, and a smaller step size (beginning slightly further out than the final terms so as to give some overlap with the initial estimate and check the consistency of the estimates) in order to fully reconstruct the metric function.

In any case, the more exotic spacetimes one might wish to consider may not have only one independent metric function $f(r)$ to extract, and in order to fully determine the metric in these more general cases, one may also need to consider the use of null geodesic probes. Thus having now established the principles of the method, and seen some examples, we go on to look at comparisons with an alternative method of extracting the bulk metric proposed in previous work.

4 Comparison with an alternative approach to metric extraction

After seeing in the previous section examples of how the extraction works in practice, we now consider how this method (S) based on spacelike geodesics compares to an alternative method involving null geodesics (N). Before we do so, however, we firstly provide a short review of this different approach to probing the bulk, which was originally presented in [10].

4.1 Review of the null geodesic extraction method

For a spacetime of the form of (1) with metric function $f(r)$ as in (18) say, we can consider the full set of null geodesic paths through the bulk, which is obtained by choosing some arbitrary starting point on the boundary and varying the ratio, $y = J/E$ from zero to one, see figure 11

From this plot of the endpoints, if one takes the gradient $dt/d\phi$ at any point, one

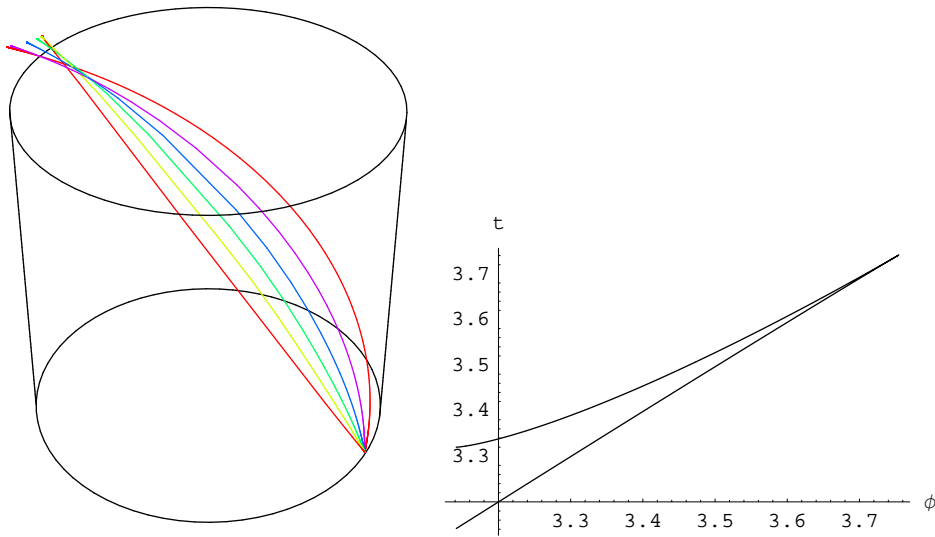


Fig. 11: Null geodesic paths passing through a modified AdS spacetime, all starting from the arbitrary point $t = 0$, $\phi = 0$ on the boundary and with $y > 0$. The corresponding full spectrum of null geodesic endpoints for this spacetime is shown on the right. (Redrawn figure from [10])

obtains the value of y for the corresponding geodesic. This is in a sense the “extra” piece of information (analogous to considering $d\mathcal{L}/d\phi$, see section 3.1) determined from the CFT which allows the geodesic probes to extract the bulk metric; here it is the ratio y of angular momentum to energy which is obtained, in the spacelike geodesic method it was simply J . After determining the first term of the iteration by taking the spacetime to be pure AdS far away from the centre, one can then take similar approximations to those given in Appendix A to split up the relevant geodesic equation:

$$\int_{t_0}^{t_1} dt = 2 \int_{r_{min}}^{\infty} \frac{1}{f(r) \sqrt{1 - y^2 \frac{f(r)}{r^2}}} dr \quad (23)$$

and combine with the relation $y = r_{min}/\sqrt{f(r_{min})}$ to iteratively extract the metric. At this point it is worth making a computational observation about the two approaches; both involve almost identical procedures for iteratively extracting the metric, and as such are of comparable efficiency. There are, however, a number of fundamental differences between them, as we shall now discuss.

4.2 Dimensional applicability

Whilst in [10] method N was applied to the specific case of AdS_5 , it is equally applicable in an arbitrary dimensional spacetime, AdS_{n+1} (for $n \geq 2$), assuming

one could obtain the endpoint information from the appropriate field theory on the boundary. Whilst the principles of method S can also be applied in arbitrary dimensions, it is no longer clear as to whether the proper length of the spacelike geodesic is so readily extractable from the CFT in anything other than the $n = 2$ case. In higher dimensions, the area of the minimal surface which corresponds to the entanglement entropy is no longer the length of a spacelike geodesic, and the method would need to be modified to take this into account. This could be achieved either by using some expression for the minimal surface instead of the proper length equation (10), or by demonstrating an alternative route to determining the proper length.

4.3 Singular spacetimes and those with significant deviation from pure AdS

One of the main limitations of method N is that it cannot probe past a local maximum in the effective potential for the null geodesics (see figure 12); it cannot therefore probe close to the horizon of a black hole for instance. The method presented here would have no such problem, as the spacelike geodesics can reach arbitrarily close to the horizon while still being able to return to the boundary. For example, consider a five dimensional Schwarzschild-AdS spacetime with metric function $f(r)$ given by:

$$f(r) = 1 + r^2 - \frac{2}{r^2} \quad (24)$$

where we have set $r_h = R = 1$. As was shown in [10], using method N one is only able to probe down to a radius of $r = 2$, as at this point the effective potential for the null geodesics becomes a local maximum. Method S, however, allows the bulk information to be fully determined all the way to the horizon radius, $r_h = 1$. Similarly, for those non-singular spacetimes with large enough deviation from pure AdS so as to allow for null geodesic orbits (the signature of a non-monotonic effective potential), one has no problem extracting the full metric using method S, as in the second and third examples of section 3.3.

4.4 The overall conformal factor

Finally, one should point out that the method presented here is also sensitive to the overall conformal factor of the metric, whereas method N is not. This simply stems from the fact that for null geodesics, ds^2 is zero, and hence for any metric:

$$ds^2 = \Omega(r) \left(-f(r)dt^2 + \frac{dr^2}{f(r)} + r^2d\phi^2 \right) \quad (25)$$

the conformal factor immediately drops out. For spacelike geodesics however, $ds^2 = 1$, and thus the $\Omega(r)$ term remains. Whilst this conformal factor $\Omega(r)$ presents us with another unknown, we shall see in the following section how it can be determined by combining the two methods (N and S) together.

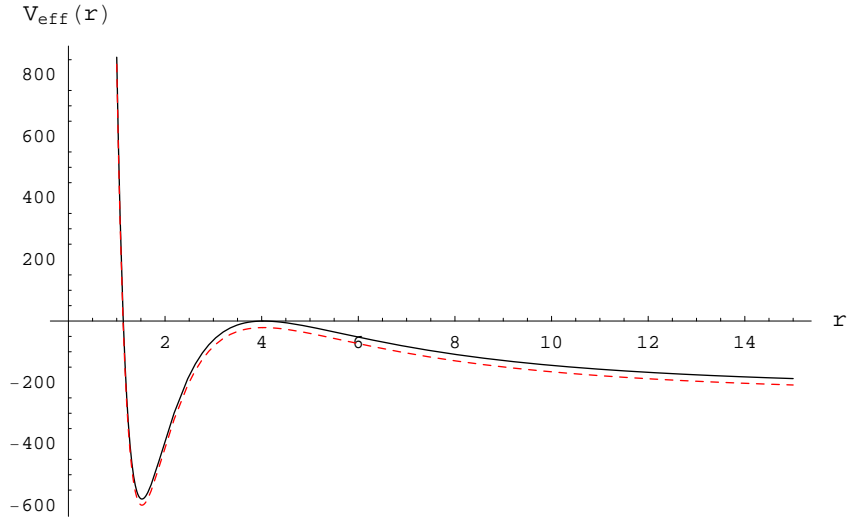


Fig. 12: Plot of the effective potential for two null geodesics with similar y , in some arbitrary spacetime. The null probe which follows the solid effective potential will go into circular orbit due to the local maximum; the geodesic with slightly lower y (dashed red line) then has significantly lower r_{min} , and this finite jump in the minimum radius causes the iterative extraction method to break down.

5 Applying the two methods together

Having compared the relative merits of the two methods, we now investigate how it is possible to use them in conjunction with one another to determine the metric in more general cases. Thus far we have restricted ourselves to considering metrics of the form of (1), however, we can look to extend this further by considering the most general static, spherically symmetric spacetimes, given by metrics of the form:

$$ds^2 = -f(r)dt^2 + h(r)dr^2 + r^2d\phi^2 \quad (26)$$

where we have incorporated the conformal factor $\Omega(r)$ of (25) into two new functions $f(r)$ and $h(r)$ (and rescaled the radial coordinate accordingly). Using either method independently to recover the metric fails because of the presence of three unknowns: r , $f(r)$, and $h(r)$ with only two independent equations with which to determine them. We can, however, use both methods in conjunction, as outlined below, where we restrict ourselves to the (2+1)-dimensional case in accordance with section 4.2.

For a spacetime of the form of (26), we have the two constraints on the energy and angular momentum from before:

$$E = f(r)\dot{t} \quad (27)$$

$$J = r^2\dot{\phi} \quad (28)$$

along with the modified expression involving the effective potential:

$$\dot{r}^2 - \left(\frac{\kappa}{h(r)} + \frac{E^2}{f(r)h(r)} - \frac{J^2}{h(r)r^2} \right) = 0 \quad (29)$$

We immediately see that for the zero energy spacelike geodesic paths we do not obtain any information about the function $f(r)$ (as we would expect, as $f(r)$ affects the time coordinate, which is kept constant in the $E = 0$ case), and our integrals for the separation of the endpoints and proper length are given by:

$$\phi_{end} - \phi_{start} = 2 \int_{r_{min}}^{r_{max}} \frac{\sqrt{h(r)}}{r\sqrt{\frac{r^2}{J^2} - 1}} dr \quad (30)$$

and

$$\mathcal{L} = 2 \int_{r_{min}}^{r_{max}} \frac{\sqrt{h(r)}}{\sqrt{1 - \frac{J^2}{r^2}}} dr \quad (31)$$

We can thus use the static spacelike geodesics to determine $h(r)$, from $r = 0$ to an arbitrarily large r_n , by applying the extraction method proposed in section 3 and Appendix A. Specifically, for each r_i we have the corresponding $h(r_i)$, and from this one can generate a best fit curve, $h_{fit}(r)$. One then is left with extracting the $f(r)$ information from the null geodesic endpoints: for a null geodesic in a bulk with metric (26), we have that

$$\int_{t_{start}}^{t_{end}} dt = 2 \int_{r_{min}}^{\infty} \frac{\sqrt{h(r)}}{f(r)\sqrt{\frac{1}{f(r)} - \frac{y^2}{r^2}}} dr \quad (32)$$

with the minimum radius given by $y = r_{min}/\sqrt{f(r_{min})}$. If we now replace the function $h(r)$ with our estimate $h_{fit}(r)$, this becomes

$$\int_{t_{start}}^{t_{end}} dt = 2 \int_{r_{min}}^{\infty} \frac{\sqrt{h_{fit}(r)}}{f(r)\sqrt{\frac{1}{f(r)} - \frac{y^2}{r^2}}} dr \quad (33)$$

which contains only two unknowns, as the parameter y is given by the gradient of the endpoints (see section 4.1). We can then use the iterative method of [10] (the relevant equations are given in Appendix C) to recover the second metric function, $f(r)$, and the bulk information has been extracted, as we see for the two examples which follow. The main area of concern would be whether significant errors in recovering $f(r)$ appear unless the estimate function for $h(r)$ is highly accurate; one can investigate whether this is so by running the extraction of $f(r)$ several times using a different estimate for $h(r)$ each time. We see how this affects the results in the first example below. Finally, one should note that the depth to which the metric can be recovered is subject to the same restrictions as before (see section 4.3): for example in singular spacetimes, whilst the spacelike geodesics can probe

down to the horizon radius, r_h (and we thus obtain $h(r)$ down to $h(r_h)$), the null geodesics can only probe as far as the first local maximum in the effective potential (figure 12), at some $r_{h2} > r_h$, leaving $f(r)$ undetermined for $r < r_{h2}$. Nevertheless, by combining the two different approaches to probing the bulk, we have obtained more information than is possible using either individually.

5.1 Example 1: Testing the combined extraction procedure

Consider a spacetime where the two metric functions $f(r)$ and $h(r)$ are given by the following:

$$f(r) = 1 + r^2 - \frac{7r^2}{(r^2 + 1)(r^2 + 13)} + \frac{2r \sin(5r)}{r^4 + 15} \quad (34)$$

$$h(r) = \left(1 + r^2 - \frac{4r^2}{(r^2 + 1)(r^2 + 8)} + \frac{3r \sin(2r)}{r^4 + 1} \right)^{-1} \quad (35)$$

Whilst this is in no way meant to be a representation of any physical deformation of the bulk, it is a good test of the combined extraction method, as it provides a monotonic effective potential for the null geodesics, and so allows us to probe down to $r = 0$. One can also use the similarity between this spacetime and that described in the first example of section 3.3, namely that we have $h(r) = f_1(r)^{-1}$. This was deliberately chosen so the part of the metric probed by the spacelike geodesics is exactly as it was in the case of example 1; the change in $f(r)$ has no effect on the results, and thus the best fit estimates for $h(r)$ are exactly those specified by the values of the parameters in Table 1. We therefore have four different estimates for $h(r)$ (one for each of the four choices of step size used), and we label them $h_{0.1}(r)$ through to $h_{0.005}(r)$, where the subscript refers to the step size. All that is left to do is to attempt to recover $f(r)$ via the null geodesic data⁹ for each fit to $h(r)$, and compare it firstly to the actual values, and also to those obtained using the exact function $h(r)$ rather than an estimate. The results are analyzed using a best fit of the form of (21) and are presented in Table 4.

We see quite clearly from the table of results that even using our roughest estimate for $h(r)$, namely $h_{0.1}(r)$, we obtain a highly accurate estimate for $f(r)$. Indeed, the limiting factor is not the accuracy of the estimate for $h(r)$, rather it is the choice of step size and starting y in the null geodesic part of the extraction (see footnote 9).

5.2 Example 2: Radiation in AdS_3 , a toy model

As the two extraction methods give such good fits when applied sequentially, we now turn our attention to a less trivial example, where we consider a gas of radi-

⁹As we saw in [10], one can use a range of different step sizes in y to obtain varied levels of accuracy in the metric extraction; as we are not intending to specifically analyze the null geodesic method here, we simply choose a starting value of $y = 0.9985$, and a step size of $\Delta y = 0.0005$, as these are sensible values for the example given.

$h_{\text{fit}}(r)$	α (7)	β (1)	γ (13)	χ (2)	η (5)	λ (15)
$h_{0.1}(r)$	6.81	1.03	12.49	2.00	4.99	14.92
$h_{0.05}(r)$	6.81	1.03	12.48	2.00	4.99	14.92
$h_{0.01}(r)$	6.80	1.03	12.48	2.00	4.99	14.92
$h_{0.005}(r)$	6.80	1.03	12.48	2.00	4.99	14.92
$h(r)$	6.80	1.03	12.48	2.00	4.99	14.92

Table 4: Best fit values (to 2 d.p.) for the $f_{\text{fit}}(r)$ parameters α , β , γ , χ , η and λ , with the actual values indicated in brackets. We see that even our roughest estimate for $h(r)$ is close enough for the extraction of $f(r)$ to be highly accurate.

ation in AdS_3 . There have been numerous papers exploring this and other closely related geometries in various dimensions, such as [11, 12, 13, 14], and we focus here purely on our ability to recover the metric information via our numerical extraction methods. Firstly, we note that whilst restricting ourselves to three bulk dimensions does make our spacelike geodesic method fully applicable (see section 4.2), it also restricts the physical realism of the model due to the non-dynamical nature of gravity. Nevertheless, it provides a good toy model for radiating “stars” in AdS spacetimes, and allows us to demonstrate how well the pertinent information (e.g. the “star’s” mass and density profiles) about the bulk can be recovered. We consider a perfect fluid solution to Einstein’s equations, with the pressure $P(r)$ set equal to half the density, $\rho(r)/2$, as for radiating matter the stress-energy tensor is traceless. For a metric of the form of (26), we find that¹⁰:

$$h(r) = (1 + r^2 - m(r))^{-1} \quad (36)$$

and

$$f(r) = \left(\frac{\rho_\infty}{\rho(r)} \right)^{2/3} \quad (37)$$

where the mass function is defined by:

$$m(r) = 2 \int_0^r \rho(\hat{r}) \hat{r} \, d\hat{r} \quad (38)$$

and ρ_∞ is the leading coefficient of $\rho(r)$ at large r , and is given by $\rho_\infty \approx \rho(r)r^3$ as $r \rightarrow \infty$. We obtain from the field equations a pair of coupled ODEs for $m(r)$ and $\rho(r)$:

$$m'(r) = 2\rho(r)r \quad (39)$$

$$\frac{6 + 3\rho(r)}{1 + r^2 - m(r)} + \frac{2\rho'(r)}{\rho(r)r} = 0 \quad (40)$$

¹⁰We set $R = 1$ and $8\pi G_3 \equiv 1$ for convenience.

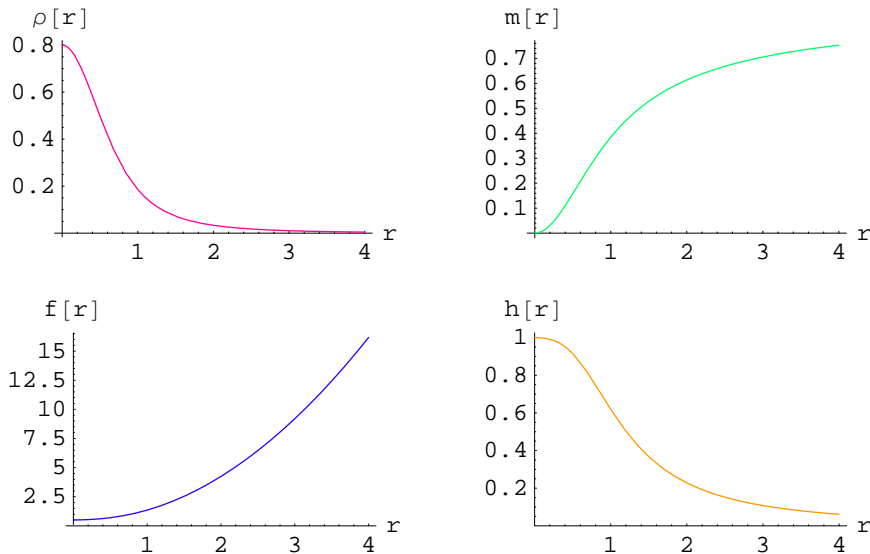


Fig. 13: The density and mass profiles (top plots) for a “star” with central density $\rho_0 = 0.8$, along with plots of the corresponding metric functions $f(r)$ and $h(r)$ (bottom).

which when combined with the relevant boundary conditions $m(0) = 0$ and $\rho(0) = \rho_0$ can be numerically solved to allow us to generate the geometry of the spacetime (see figure 13). The condition $\rho(0) = \rho_0$ specifies the internal density of the gas, and ρ_0 is the single free parameter of the system: pure AdS is recovered when $\rho_0 = 0$.

Before we begin with the metric extraction, we should make a comment about the features of such spacetime at large radius, as there are significant differences in the asymptotic behaviour of the metric depending on the choice of ρ_0 . For $\rho_0 \neq 0$, we have that the asymptotic behaviour of the metric functions is given by

$$h(r) \rightarrow (1 + r^2 - M)^{-1} \quad \text{and} \quad f(r) \rightarrow 1 + r^2 - M \quad \text{as } r \rightarrow \infty \quad (41)$$

where $M > 0$ is a constant. If $M > 1$ we have that the metric becomes the BTZ black hole solution at large r (see [15, 16, for example] for more details); this poses a problem for the method involving null geodesics, as we can no longer use them to probe the full range of r . Whilst this is due to the form of the effective potential (see figure 14), it is not due to the local maximum problem we saw in section 4.3. Rather here we no longer have geodesics which can usefully probe the spacetime *away* from the centre: for the full set of null geodesics (obtained by varying y from zero to one), the minimum radius reached by the geodesics is bounded from above. We thus cannot take r_{min} to be arbitrarily large on the first step of our iteration, which was necessary for us to begin extracting the metric (although we should note that we could still apply the spacelike method to extract $h(r)$ in this scenario). Instead however, we will consider the region $0 < M < 1$, corresponding to conical

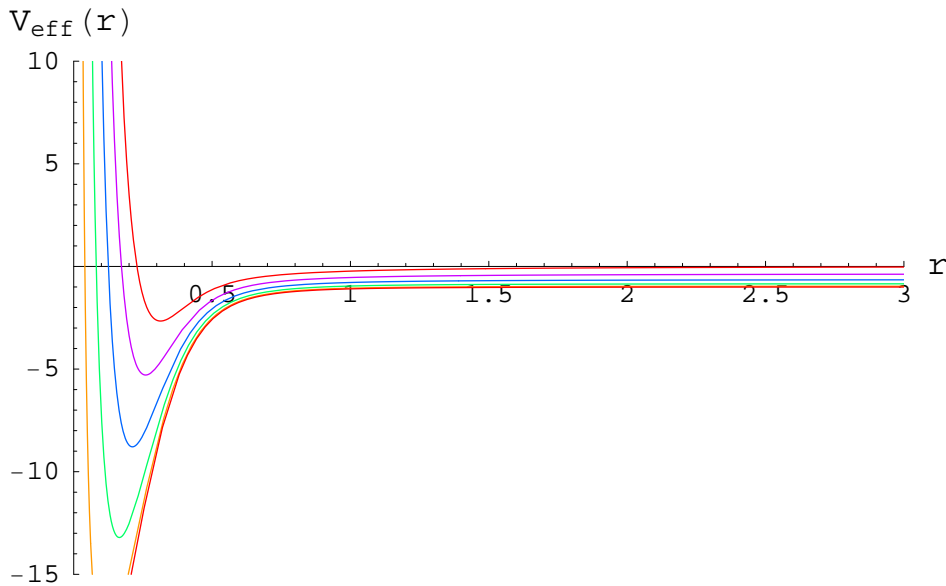


Fig. 14: Effective potentials for null geodesics in a spacetime with $M = 8$. The upper (red) potential is for $y \equiv J/E = 0.9999$; no matter how close to one the ratio J/E becomes, the minimum radius (defined by $V_{eff} = 0$) remains small.

defects, in which both methods are applicable and is obtained by taking ρ_0 to be small.¹¹

Let us then proceed with recovering the metric in the specific example shown in figure 13, where we have set $\rho_0 = 0.8$. Bearing in mind that our goal is to firstly reconstruct the functions $f(r)$ and $h(r)$, and then use these to determine the mass and density profiles ($m(r)$ and $\rho(r)$ respectively) of the star, we begin by applying the spacelike geodesic method (with step sizes of 0.1, 0.05 and 0.01) to produce three estimates for $h(r)$, the most accurate of which, namely $h_{0.01}(r)$, is shown in figure 15. Whilst in the previous example we defined $h(r)$ explicitly by hand, and so knew the form of the function with which to apply the non-linear fit to generate the best fit curve $h_{fit}(r)$, here we do not have such a starting point. Instead, we use the data points $(r_{n-i}, h(r_{n-i}))$ to generate an interpolating function which will serve as our $h_{fit}(r)$. Thus although we cannot write down an explicit form for $h_{fit}(r)$, we can use the interpolating function to then carry out the next part of the extraction process, namely using the null geodesic probes to recover $f(r)$.

Using the third (and most accurate) estimate for $h(r)$ in the modified null geodesic method of section 5 and Appendix C, we produce the estimate for $f(r)$,

¹¹One should also note from (41) that our iterative equations for recovering the metric need to be modified to take into account the new asymptotic behaviour, as we no longer have that the metric is given by $f(r) \approx r^2 + 1$ at large r . Thus we say that for $r \geq r_n$ we have that $f(r)$ and $h(r)$ are given by (41), and modify the approximations to the integrals for ϕ_{n-i} and \mathcal{L}_{n-i} accordingly.

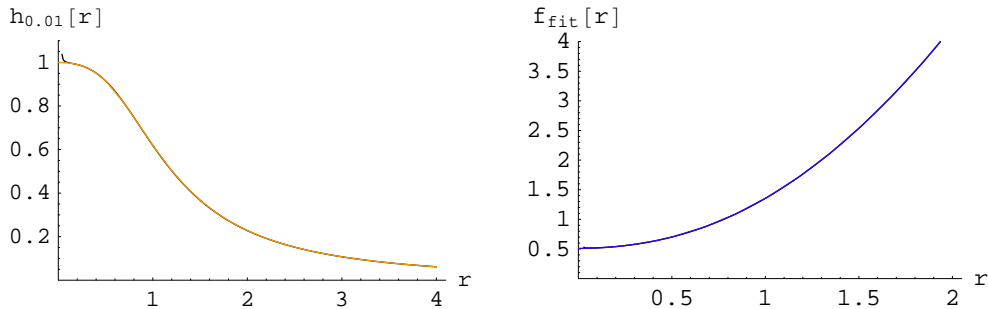


Fig. 15: The third (and most accurate) estimate for $h(r)$, where the fit is good down to $r \sim 0.1$ (left plot). The estimate for $f(r)$ generating using this approximation to $h(r)$ is given in the right plot, and we see that it too appears accurate down to very low r .

$f_{fit}(r)$, also shown in figure 15: we have now reconstructed the star metric. Although if we so wished we could have taken smaller step sizes to improve both the estimate of $h(r)$ and that of $f(r)$, we now continue with the ones we have.

How do we use the metric functions to determine the mass and density information for the star? From (36) it is immediately obvious: we can rearrange the equation to solve for $m(r)$, and substitute in our interpolating function $h_{fit}(r)$ to give an estimate for the mass profile:

$$m_{fit}(r) = 1 + r^2 - \frac{1}{h_{fit}(r)} \quad (42)$$

and we obtain a fit for the density profile in similar fashion, by using the above estimate for $m(r)$ in (39), to give:

$$\rho_{fit}(r) = \frac{m'_{fit}(r)}{2r} \quad (43)$$

These two fits are plotted against the actual functions $m(r)$ and $\rho(r)$ in figure 16, and we see that by using the metric function data $h_{fit}(r)$ we have obtained reasonably good estimates of the mass and density profiles of the star, aside from at very small r , where the errors from the estimate of $h(r)$ become noticeable. What is noticeable is that the estimate for $\rho(r)$ fails at higher r than any of the others; this is due to the use of the derivative of the interpolating function $m_{fit}(r)$ in its construction, and is dealt with later (see below).

One now asks the obvious question of why it was necessary to extract the function $f(r)$ at all, seeing as we have apparently just reconstructed the information about the star simply by using $h_{fit}(r)$. This is where we recall that we should be assuming that *a priori* we knew nothing about the origin of the metric's deviation from pure AdS. In fact, this has not been the case. Whilst our expressions for $h(r)$ in terms of $m(r)$ and the mass $m(r)$ in terms of the density $\rho(r)$, (36) and (39), stem from

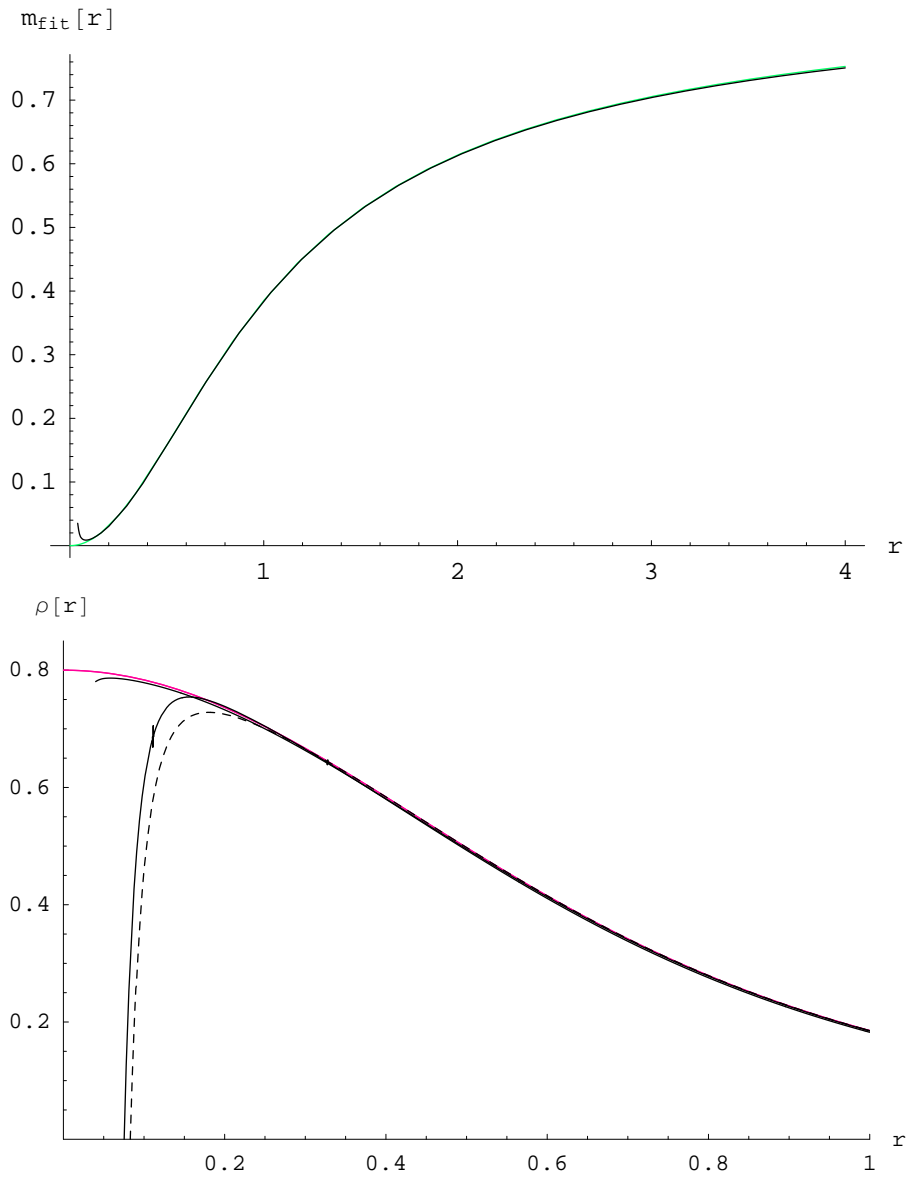


Fig. 16: Estimates for the mass and density profiles for our “star”. As with $h_{0.01}(r)$ and $f_{\text{fit}}(r)$, these match the actual curves closely until low r , although the density estimate $\rho_{\text{fit}}(r)$ (dashed) fails at noticeably higher r than the others. Included in the lower plot are alternative estimates for for the density profile, obtained from (37) (closest fit) and (44) (solid)

the dimensionality of the bulk (e.g. in higher dimensions one would have the $m(r)$ term multiplied by some negative power of r), in defining $f(r)$ by (37) we have already taken the matter content to be a gas of radiation, which sets $P(r) = \rho(r)/2$ and removes the pressure profile as an unknown. Given this knowledge, one could indeed have simply used the spacelike geodesic method say to extract the information about the star, as $h(r)$ gives $m(r)$, and $m(r)$ gives $\rho(r)$. Extracting $f(r)$ becomes a necessity, however, if one removes the assumption about the matter content; then one also has to compute the pressure profile. It is most easily determined (once we have our fits for $f(r)$ and $h(r)$) from the G_{rr} component of Einstein's equations, and we have that:

$$P_{\text{fit}}(r) = \frac{f'_{\text{fit}}(r)}{2r f_{\text{fit}}(r) h_{\text{fit}}(r)} - 1 \quad (44)$$

which in our example corresponds to $\rho_{\text{fit}}(r)/2$. Therefore by also plotting $2P_{\text{fit}}(r)$ in figure 16, we can see how close the fits generated by the two different expressions (43) and (44) match, and this provides a check that the matter content is indeed that of a gas of radiation and confirms that our expression, (37), for $f(r)$ is correct. Interestingly, we see that this expression provides a slightly better fit to $\rho(r)$ at small r than that from (43). This is simply because (44) includes $f_{\text{fit}}(r)$ terms, and the non-linear step size in r in the null extraction method generates a greater amount of data points at low r for the estimate for $f(r)$, thus allowing the derivative of the interpolation function to be more accurately determined. We can obtain the best fit at low r by using $f_{\text{fit}}(r)$ in (37) and solving for $\rho(r)$ (see figure 16), where we have avoided using derivatives.¹²

Finally, we can use the estimates to give a numerical value for our free parameter ρ_0 . Taking ρ_∞ as having been calculated from the asymptotic fall off, and approximating the value of $f(0)$ as 0.525, we obtain a value of 0.76, compared with the actual value of $\rho_0 = 0.8$. Whilst the match is fairly good, this is where the accuracy of the estimates for $f(r)$ and $h(r)$ become very important; in taking $f(0) = 0.525$ we have discarded the final few iterations of $f_{\text{fit}}(r)$ at small r , which lead to a kink in the curve, as being erroneous and due to an incomplete recovery of $h(r)$. This is a reasonable assumption to make, as in our previous examples we saw that for too large a step size the method of generating $h_{\text{fit}}(r)$ fails to reach down to $r = 0$. We also have the data from the higher step size fits ($h_{0.1}(r)$ and $h_{0.05}(r)$) with which to analyse the accuracy of our estimates for $h(r)$ at low r . However, as it is the small r region from which the numerical value of ρ_0 is calculated, in order for it to be confidently extracted one must ensure the estimates $h_{\text{fit}}(r)$ and $f_{\text{fit}}(r)$ are thoroughly checked for r close to zero.

¹²One should note this does firstly require the value of ρ_∞ to be determined from the fall off of $\rho(r)$ at large r ; this is however available from our earlier fit to ρ given in (43).

6 Extensions to less symmetric cases

In all of the above we have taken the spacetime metric to be both static and spherically symmetric, however, we now consider how the methods for extracting the bulk presented here could be extended to include more general cases.

Reducing the amount of symmetry removes conserved quantities from the geodesics; spherical symmetry gives us conservation of angular momentum, time translational symmetry gives us energy conservation. Consequently, there will be additional unknowns introduced in our analysis of the geodesic path, as we will need to know more details about its route through the bulk; this should not prove a problem, however, as there will also be further information available from the geodesic equations.

Consider for example the non-spherically symmetric (but still static) case. Before, when there was no angular dependence in the metric, we considered a series of geodesics which probed deeper and deeper into the bulk - in other words, we had one which probed down to each r_{n-i} . These were specified by the angular separation of the endpoints on the boundary, and the actual values of the ϕ_{start} and ϕ_{end} were unimportant. This allowed us to reconstruct the bulk step by step, one value of $f(r_{n-i})$ at a time.

Now, what is the analogous method in the non-spherically symmetric case? At each step of the iteration we can still consider some fixed angular separation of the endpoints, however, we must also vary ϕ_{start} from 0 to 2π (with some choice of slicing sufficient to give an accurate estimate), such that for each iterative step we recover a “ring” of information about the metric. The subsequent steps then recover smaller and smaller rings, extracting the metric function down to the centre of the spacetime. This is the basic idea of the extraction method; finalising a more detailed procedure which gives high accuracy within a reasonable computational time is subject of current research, one now has two step sizes to consider: the slicing in ϕ and the radial steps in r .

Finally, we should recall that higher dimensional cases offer further complications, as mentioned in section 4.2, as although the null geodesic method is already applicable in such cases, the spacelike method is not. In principle though, the ideas still hold; one would need an expression for the correct minimal surface corresponding to the entanglement entropy (see [9] for more details on this point) which could then be treated in much the same way as the geodesic proper length, as they will each probe to a certain depth in the bulk, and those remaining at large r will behave as in pure AdS. Completing the analysis for these cases is again the subject of further research.

7 Discussion

In this paper we have seen how the bulk geometry can be extracted (in asymptotically Anti-de Sitter spacetimes) using the entanglement entropy information obtained from the corresponding boundary field theory. In the three dimensional case,

the entanglement entropy of a subsection A of the $1 + 1$ dimensional boundary is proportional to the proper length of the static spacelike geodesic connecting the endpoints of A (see figure 2). Using this relation, (6), together with the endpoint data allows both the minimum radius, r_{min} , of the spacelike geodesic and the value of the metric function $f(r_{min})$ at this point to be determined, provided sufficient information about the bulk is known for $r > r_{min}$. Thus by starting from large r , where the metric is approximately pure AdS, one can probe further and further into the bulk using geodesics connecting progressively smaller regions on the boundary.

This extraction of the metric is made significantly more straightforward by an interesting relationship between the proper length of the geodesic and the angular separation of its endpoints. Specifically, the gradient, $d\mathcal{L}/d\phi$, gives the angular momentum, J , of the corresponding geodesic, which in the static, spherically symmetric cases considered here, is equal to the minimum radius the geodesic probes down to in the bulk.

An iterative method for recovering the metric information in practice by approximating the relevant geodesic equation was thus then proposed, and a number of examples were given. The iterative method was developed in analogous way to the method presented in [10], which used the endpoint data of null geodesics to similarly extract the bulk information, and was reviewed in section 4.1.

A comparison of the two methods was then made, investigating their relative advantages and disadvantages; this highlighted a number of differences in their relative applicabilities. Whilst the method of [10], which uses null geodesics as probes, runs into problems when encountering geometries with significant deviation from pure AdS (as this leads to a non-monotonic effective potential for the geodesics which limits the depths to which the metric information can be recovered), no such limitations arise for the method given here involving spacelike geodesics, unless the metric is also singular. On the other hand, the null geodesic method is completely applicable in any number of dimensions, whereas although the principle of extracting the metric via spacelike geodesics can be extended to greater than three bulk dimensions, the relation between entanglement entropy and minimal surface area (6) no longer involves the geodesic's proper length, and thus this quantity is no longer so readily available from the CFT. Computationally, the two methods (as presented here) are of comparable efficiency, although both have scope for further optimization.

Significantly, we demonstrated in section 5 how the two methods can be applied together to allow the probing of the most general static, spherically symmetric asymptotically AdS spacetimes, with metric of the form of (26). This is a notable extension to the applicability of either method individually, as whilst part of the metric information (i.e. the $h(r)$ of (26)) could always be extracted using the spacelike geodesics, they could never give any insight into $f(r)$. The null geodesics, on the other hand, can probe both $f(r)$ and $h(r)$ but without yielding enough information to determine either, without some *a priori* knowledge of a relationship between them. It is the separation of the two functions in the spacelike case, however, which allows the methods to be combined so straightforwardly, as one firstly determines

an estimate for $h(r)$, then takes this as a known function when analyzing the null geodesic data. We concluded by considering the toy model scenario of a gas of radiation (a “star”) in AdS_3 and demonstrated how the recovery of the metric allowed the pertinent information of the star (its mass and density profiles) to be well estimated. Whilst the estimates produced were accurate down to low r (dependent on the choice of step size in both the null and spacelike methods), one had to be careful when using the derivative of $m_{\text{fit}}(r)$ (the interpolating fit to the mass profile) to generate $\rho_{\text{fit}}(r)$. Although the fit produced was still good, it failed at noticeably larger r than the fits for any of the other functions, due to inaccuracies introduced via $m'_{\text{fit}}(r)$. This could be avoided by using the alternative definition of $\rho(r)$ in terms of $f(r)$, (37), provided one first extracted the asymptotic fall off of the density as $r \rightarrow \infty$.

Finally, we noted in section 6 that this work can be extended further by considering spacetimes which are not spherically symmetric, and by investigating the higher dimensional cases where the area of the minimal surface relating to the entanglement entropy is not simply the length of the corresponding static spacelike geodesic. Both avenues have the prospect of yielding fruitful results for metric computation in AdS/CFT. Also, one could approach the problem of metric extraction from a different angle, by investigating whether there are alternative methods available which do not involve the use of geodesic probes. If so, it would be interesting to see whether these lead to more efficient ways of computing the metric functions than those described here.

Acknowledgements

For useful discussions and feedback I wish to thank Veronika Hubeny (who also provided much encouragement and helpful information) along with Simon Creek, Martyn Gigg, Elizabeth Holman, Kemal Ozeren and James Umpleby. This work was supported by an EPSRC studentship grant and the University of Durham Department of Mathematical Sciences.

Appendix A

In section 3 we outlined the principle behind the iterative technique of metric extraction: determining r_{min} from the gradient $d\mathcal{L}/d\phi$ and then calculating an estimate for $f(r_{\text{min}})$ at each step by splitting up the integral in (66) and approximating each piece separately, beginning the whole process at large r , where the metric is approximately pure AdS and we can take $f(r) \approx r^2 + 1$. Here we go on to give further details of how to set this up, and explicitly write down the equations used in the approximations¹³.

¹³The procedure used here is only one of a number of possible methods for discretizing the integral; for the purposes of illustrating the principle, this method is both brief and accurate to a good degree.

Having taken the first step which chooses an r_n large enough so the metric is approximately pure AdS, and hence $f(r_n) = r_n^2 + 1$, we can continue as follows. For a geodesic with slightly lower angular momentum J_{n-1} (which can be obtained by taking a slightly larger region B on the boundary), we can split up the integral over r in (9) into two pieces:

$$\phi_{n-1} = 2 \int_{r_{n-1}}^{r_n} \frac{1}{r \sqrt{f(r)} \sqrt{\frac{r^2}{J^2} - 1}} dr + 2 \int_{r_n}^{r_{max}} \frac{1}{r \sqrt{f(r)} \sqrt{\frac{r^2}{J^2} - 1}} dr \quad (45)$$

The first integral in the above can be well approximated by taking a next-to-lowest order series expansion about the point $r = r_{n-1}$ ($= J_{n-1}$), as the distance $r_n - r_{n-1}$ is small. For the second integral, we can again use our assumption that $f(r) = r^2 + 1$ for $r \geq r_n$, and overall we obtain for the angular separation of the endpoints:

$$\begin{aligned} \phi_{n-1} \approx & 2\sqrt{2} \sqrt{\frac{r_n - r_{n-1}}{r_{n-1} f(r_{n-1})}} - \frac{5f(r_{n-1}) + 2r_{n-1}f'(r_{n-1})}{3\sqrt{2}} \left(\frac{r_n - r_{n-1}}{r_{n-1} f(r_{n-1})} \right)^{3/2} \\ & + \arctan \left(\frac{2r_{n-1}^2 + (r_{n-1}^2 - 1)r_n^2}{2r_{n-1} \sqrt{r_n^4 - (r_{n-1}^2 - 1)r_n^2 - r_{n-1}^2}} \right) \\ & - \arctan \left(\frac{r_{n-1}^2 - 1}{2r_{n-1}} \right) \end{aligned} \quad (46)$$

where we have again taken the limit $r_{max} \gg r_n > r_{n-1}$. Alternatively, one could perform similar approximations on the equation for the proper length, (10), to obtain:

$$\begin{aligned} \mathcal{L}_{n-1} \approx & 2\sqrt{2r_{n-1}} \sqrt{\frac{r_n - r_{n-1}}{f(r_{n-1})}} + \frac{3f(r_{n-1}) - 2r_{n-1}f'(r_{n-1})}{3\sqrt{2}r_{n-1}} \left(\frac{r_n - r_{n-1}}{f(r_{n-1})} \right)^{3/2} \\ & + 2 \log(2r_{max}) - 2 \log \left(\sqrt{r_n^2 - r_{n-1}^2} + \sqrt{r_n^2 + 1} \right) \end{aligned} \quad (47)$$

In the above expressions we have introduced a further unknown, namely the gradient of the function $f(r)$ at the point $r = r_{n-1}$; this can be eliminated by taking the simple linear approximation:

$$f'(r_{n-1}) \approx \frac{f(r_n) - f(r_{n-1})}{r_n - r_{n-1}} \quad (48)$$

which holds provided the radial distance $r_n - r_{n-1}$ is kept small.¹⁴ As we mentioned in section 2.1, we can calculate the proper length \mathcal{L}_{n-1} from the relevant entanglement entropy expression, in general this is given by:

¹⁴The presence of an $f'(r)$ term deserves further comment: one can avoid introducing it by using the lowest order expansion, however, this reduces the overall accuracy of the method. The

$$\mathcal{L} = 4G_N^{(3)} S_A \quad (49)$$

where S_A corresponds to the entanglement entropy for the subsystem A in the deformed spacetime. Taking the entanglement entropy as a known quantity from the CFT, along with the angular separation of the endpoints (which is given simply from the length of the subsystem in the CFT) one can calculate the corresponding minimum radius r_{n-1} from (17), and so our only remaining unknown in both (46) and (47) is $f(r_{n-1})$. We can thus numerically solve either for $f(r_{n-1})$, and determine the metric function at this point. Continuing in a similar fashion, by taking geodesics with progressively smaller angular momenta and numerically solving at each step, we can iteratively extract the complete metric. For general ϕ_{n-i} and \mathcal{L}_{n-i} the integrals are split up into $(i+1)$ pieces; two are approximated as in (46) and (47), with the remaining terms evaluated using Simpson's rule (a polynomial fit to the curve). The general expression for ϕ_{n-i} can then be written as:

$$\phi_{n-i} \approx A_{n-i} + B_{n-i} + C_{n-i} \quad (50)$$

where

$$A_{n-i} = 2\sqrt{2} \sqrt{\frac{r_{n-i+1} - r_{n-i}}{r_{n-i} f(r_{n-i})}} - \frac{5f(r_{n-i}) + 2r_{n-i}f'(r_{n-i})}{3\sqrt{2}} \left(\frac{r_{n-i+1} - r_{n-i}}{r_{n-i} f(r_{n-i})} \right)^{3/2} \quad (51)$$

$$C_{n-i} = \arctan \left(\frac{2r_{n-i}^2 + (r_{n-i}^2 - 1)r_n^2}{2r_{n-i}\sqrt{r_n^4 - (r_{n-i}^2 - 1)r_n^2 - r_{n-i}^2}} \right) - \arctan \left(\frac{r_{n-i}^2 - 1}{2r_{n-i}} \right) \quad (52)$$

are the two approximations we had before, and the B_{n-i} term is given by:

$$B_{n-i} = \sum_{j=1}^{i/2} \frac{(r_{n-2j+3} - r_{n-2j+1})}{3} (g_{n-i}(r_{n-2j+3}) + 4g_{n-i}(r_{n-2j+2}) + g_{n-i}(r_{n-2j+1})) \quad (53)$$

for i even¹⁵, and by

$$B_{n-i} = \sum_{j=1}^{(i-1)/2} \frac{(r_{n-2j+2} - r_{n-2j})}{3} (g_{n-i}(r_{n-2j+2}) + 4g_{n-i}(r_{n-2j+1}) + g_{n-i}(r_{n-2j})) \quad (54)$$

detrimental effect of the approximation to the gradient on the accuracy of the estimates is not as pronounced as in the method of [10] due to the use of linear step size in J (and hence r), see section 3.3. Surprisingly, an alternative integral one might consider when setting up the iteration, which allows the higher order series expansion to be used without introducing $f'(r)$, leads to an unstable method rather than a more accurate one, see Appendix B.

¹⁵Using this definition requires a value for the r_{n+1} term, which can be obtained in an identical way to that used in determining r_n

for i odd, where we have defined the function

$$g_{n-i}(r) \equiv \frac{1}{r\sqrt{f(r)}\sqrt{\frac{r^2}{r_{n-i}^2} - 1}} \quad (55)$$

for ease of notation. For the proper length we similarly have that:

$$\mathcal{L}_{n-i} \approx \mathcal{A}_{n-i} + \mathcal{B}_{n-i} + \mathcal{C}_{n-i} \quad (56)$$

with

$$\mathcal{A}_{n-i} = 2\sqrt{2r_{n-i}}\sqrt{\frac{r_{n-i+1} - r_{n-i}}{f(r_{n-i})}} + \frac{3f(r_{n-i}) - 2r_{n-i}f'(r_{n-i})}{3\sqrt{2r_{n-i}}} \left(\frac{r_{n-i+1} - r_{n-i}}{f(r_{n-i})} \right)^{3/2} \quad (57)$$

$$\mathcal{C}_{n-i} = 2\log(2r_{max}) - 2\log\left(\sqrt{r_n^2 - r_{n-i}^2} + \sqrt{r_n^2 + 1}\right) \quad (58)$$

$$\mathcal{B}_{n-i} = \sum_{j=1}^{i/2} \frac{(r_{n-2j+3} - r_{n-2j+1})}{3} (\zeta_{n-i}(r_{n-2j+3}) + 4\zeta_{n-i}(r_{n-2j+2}) + \zeta_{n-i}(r_{n-2j+1})) \quad (59)$$

for i even, and

$$\mathcal{B}_{n-i} = \sum_{j=1}^{(i-1)/2} \frac{(r_{n-2j+2} - r_{n-2j})}{3} (\zeta_{n-i}(r_{n-2j+2}) + 4\zeta_{n-i}(r_{n-2j+1}) + \zeta_{n-i}(r_{n-2j})) \quad (60)$$

for i odd, with the function ζ defined by

$$\zeta_{n-i}(r) \equiv \frac{1}{\sqrt{f(r)}\sqrt{1 - \frac{r_{n-i}^2}{r^2}}} \quad (61)$$

Thus we can continue the metric extraction down to $r = 0$ in the non-singular case, or down to $r = r_h$ in the black hole case (see section 4.3).

Appendix B

In the method of the previous appendix, the series expansion we used to approximate part of the integral in both (9) and (10) introduced an extra term, $f'(r)$, which we then chose to linearly approximate. What appears immediately obvious is that one could simply combine the two equations and avoid using any approximation to $f'(r)$ at all. Considering the two terms A_{n-i} and \mathcal{A}_{n-i} from (51) and (57) respectively, we see that:

$$r_{n-i}A_{n-i} - \mathcal{A}_{n-i} = \frac{4\sqrt{2}}{3} \frac{(r_n - r_{n-i})^{3/2}}{\sqrt{r_{n-i}f(r_{n-i})}} \quad (62)$$

and so by considering $r_{n-1} \phi_{n-1} - \mathcal{L}_{n-1}$ at each step we eliminate the $f'(r_{n-i})$ term. For completeness, we note that this is equivalent to the formulating the integral as follows: beginning with expression (16) and integrating over J gives:

$$\int^{\mathcal{L}} d\mathcal{L}' = \int J \frac{d\phi}{dJ} dJ \quad (63)$$

which can then be integrated by parts:

$$\mathcal{L}(J) = J \phi(J) - \int \phi dJ \quad (64)$$

and rewritten using the expression for ϕ from (9):

$$\mathcal{L}(J) = J \phi(J) - \int \int_{r_{min}}^{r_{max}} \frac{2}{r \sqrt{f(r)} \sqrt{\frac{r^2}{J^2} - 1}} dr dJ \quad (65)$$

We can now reverse the order of integration, and as the function $f(r)$ has no dependence on J , integrate over J . For some specific geodesic with proper length \mathcal{L}_{n-i} and angular separation ϕ_{n-i} on the boundary (to continue with the notation from earlier) we thus have that:

$$\mathcal{L}_{n-i} = r_{n-i} \phi_{n-i} + \int_{r_{n-i}}^{r_{max}} \frac{2}{\sqrt{f(r)}} \sqrt{1 - \frac{J^2}{r^2}} dr \quad (66)$$

where we have also used that $r_{min} = J$ and relabeled the minimum radius as r_{n-i} . After splitting up the integral as in Appendix A, the lowest order approximation to the integral at r_{n-i} is given by (62), and one can then seemingly determine $f(r_{n-i})$, the only unknown, for each i from one to n and hence reconstruct the entire metric function $f(r)$.

Applying this in practice, however, one immediately runs into the same stability problems that occur in the naive approach mentioned in section 3, where one attempts to recover both r_{min} and $f(r_{min})$ directly from equations (9) and (10). The method appears inherently unstable to errors, and fails to generate any reliable estimate for $f(r)$ at any step size. Interestingly, an almost identical formalism can be carried out in the method involving null geodesics (see Appendix C), however, unlike in the spacelike case, this method is both stable and highly efficient. Further analysis into what causes the stability/instability of the different methods is ongoing.

Finally, to clarify one further point, we note that the original (naive) method of section 3 can be stabilised by introducing a particular regularisation of the proper length, where one subtracts off the proper length of a corresponding geodesic in pure AdS which probes down to the same depth, r_{min} . Although this appears to not introduce any new information, one should remember that we are working from the field theory data, and as such, one does not in fact know the proper length of this geodesic, but rather the one which has the same angular separation of the

endpoints. Thus using this regularisation is actually equivalent to determining the minimum radius from (17), using this to determine the length of the corresponding geodesic in pure AdS, and then treating r_{min} as an unknown again in (50) and (56). This excessive over complication considerably reduces the efficiency of the method, as the equations are considerably more complicated to solve for (even numerically) at later steps.

Appendix C

In section 5 we combine the extraction method presented here with that given in [10]¹⁶ to allow metric recovery in the most general static, spherically symmetric spacetimes. As the methods are applied sequentially, they require very little modification in order to work together, indeed the spacelike method is only affected by the change in notation when we introduce $h(r)$. The method involving null geodesics is altered slightly more however, and so is presented in full here. This explicit presentation also serves to highlight the similarities between the two iterative procedures for extracting the metric, which is remarkable given the different origins of the field theory data.

As mentioned in the review in section 4.1, we have a relationship between the gradient of the endpoints of the null geodesics (see figure 11) and the ratio of J to E , namely $dt/d\phi = y$, which can be rewritten as:

$$\frac{dt(y)}{dy} = y \frac{d\phi(y)}{dy} \quad (67)$$

Integrating over y and then by parts gives:

$$t(y) = y \phi(y) - \int \phi dy \quad (68)$$

which can be rewritten by substituting in for ϕ :

$$t(y) = y \phi(y) - \int \int_{r_{min}}^{\infty} \frac{2y\sqrt{h(r)}}{r^2\sqrt{\frac{1}{f(r)} - \frac{y^2}{r^2}}} dr dy \quad (69)$$

Reversing the order of integration (as the function $f(r)$ has no dependence on y) allows us to integrate over y :

$$t(y) = y \phi(y) + \int_{r_{min}}^{\infty} 2\sqrt{h(r)}\sqrt{\frac{1}{f(r)} - \frac{y^2}{r^2}} dr \quad (70)$$

¹⁶There are two methods for extracting the bulk information proposed in [10]; here we proceed to adapt the second, which is noticeably more efficient in generating estimates for $f(r)$.

Thus taking the initial conditions to be $(\phi_0, t_0) = (0, 0)$, we can say that for any endpoint (ϕ_j, t_j) on the boundary we have:

$$t_j - \frac{dt}{d\phi}\Big|_{(\phi_j, t_j)} \phi_j = \int_{r_j}^{\infty} 2\sqrt{h(r)} \sqrt{\frac{1}{f(r)} - \frac{y_j^2}{r^2}} dr \quad (71)$$

where we have renamed r_{min} as r_j . After using the spacelike geodesics to determine an estimate for $h(r)$, this then finally becomes:

$$t_j - \frac{dt}{d\phi}\Big|_{(\phi_j, t_j)} \phi_j = \int_{r_j}^{\infty} 2\sqrt{h_{\text{fit}}(r)} \sqrt{\frac{1}{f(r)} - \frac{y_j^2}{r^2}} dr \quad (72)$$

which, when coupled with the equation for the minimum r ,

$$y_j^2 = \frac{r_j^2}{f(r_j)} \quad (73)$$

allows the metric function $f(r)$ to be reconstructed from the plot of the endpoints, by applying a similar iterative method to that described in Appendix A: for the general term r_{n-i} , one approximates the integral from r_{n-i} to r_{n-i+1} by the parabolic area formula; the integral from r_n to $r = \infty$ by taking the spacetime to be pure AdS; and the remaining $i - 1$ integrals by the trapezium rule, to obtain:

$$t_{n-i} - \frac{dt}{d\phi}\Big|_{(\phi_{n-i}, t_{n-i})} \phi_{n-i} \approx A_{n-i} + B_{n-i} + C_{n-i} \quad (74)$$

where

$$A_{n-i} = \frac{4}{3} (r_{n-i+1} - r_{n-i}) \eta(y_{n-i}, r_{n-i+1}) \quad (75)$$

$$B_{n-i} = \sum_{j=1}^{i-1} (r_{n-j+1} - r_{n-j}) (\eta(y_{n-i}, r_{n-j+1}) + \eta(y_{n-i}, r_{n-j})) \quad (76)$$

and

$$C_{n-i} = 2 \arctan \left(\frac{1}{\sqrt{(1 - y_{n-i}^2) r_n^2 - y_{n-i}^2}} \right) - 2 y_{n-i} \arctan \left(\frac{y_{n-i}}{\sqrt{(1 - y_{n-i}^2) r_n^2 - y_{n-i}^2}} \right) \quad (77)$$

where we have defined the function $\eta(y_j, r_k)$ as:

$$\eta(y_j, r_k) \equiv \sqrt{h_{\text{fit}}(r_k)} \sqrt{\frac{1}{f(r_k)} - \frac{y_j^2}{r_k^2}} \quad (78)$$

References

- [1] G. 't Hooft, “*Dimensional reduction in quantum gravity*”, arXiv:gr-qc/9310026.
- [2] L. Susskind, “*The World as a hologram*”, J. Math. Phys. **36**, 6377 (1995) [arXiv:hep-th/9409089].
- [3] J. M. Maldacena, “*The large N limit of superconformal field theories and supergravity*”, Adv. Theor. Math. Phys. **2**, 231 (1998) [Int. J. Theor. Phys. **38**,1113 (1999)][hep-th/9711200].
- [4] S. Ryu and T. Takayanagi, “*Holographic Derivation of Entanglement Entropy from AdS/CFT*”, arXiv:hep-th/0603001.
- [5] S. Ryu and T. Takayanagi, “*Aspects of Holographic Entanglement Entropy*”, arXiv:hep-th/0605073.
- [6] D. Fursaev, “*Proof of the Holographic Formula for Entanglement Entropy*”, arXiv:hep-th/0606184.
- [7] S. N. Solodukhin, “*Entanglement entropy of black holes and AdS/CFT correspondence*”, Phys. Rev. Lett. **97**, 201601 (2006) [arXiv:hep-th/0606205].
- [8] T. Hirata and T. Takayanagi, “*AdS/CFT and Strong SubAdditivity of Entanglement Entropy*”, JHEP **0702**, 042 (2007) [arXiv:hep-th/0608213].
- [9] V. E. Hubeny, M. Rangamani and T. Takayanagi, “*A Covariant Holographic Entanglement Entropy Proposal*”, arXiv:0705.0016.
- [10] J. Hammersley, “*Extracting the bulk metric from boundary information in asymptotically AdS spacetimes*”, JHEP **0612**, 047 (2006) [arXiv:hep-th/0609202].
- [11] V. E. Hubeny, H. Liu and M. Rangamani, “*Bulk-cone singularities and signatures of horizon formation in AdS/CFT*”, JHEP **0701**, 009 (2007) [arXiv:hep-th/0610041].
- [12] D. N. Page and K. C. Phillips, “*Selfgravitating radiation in anti-de sitter space*”, GRG (1985).
- [13] D. Astefanesi and E. Radu, “*Boson stars with negative cosmological constant*”, Nucl. Phys. **B665** (2003) 594-622 [arXiv:gr-qc/0309131].
- [14] D. Astefanesi and E. Radu, “*Rotating boson stars in $(2+1)$ dimensions*”, Phys. Lett. **B587** (2004) 7-15 [arXiv:gr-qc/0310135].
- [15] T. Banks, M. R. Douglas, G. T. Horowitz and E. J. Martinec, “*AdS dynamics from conformal field theory*”, arXiv:hep-th/9808016.

- [16] H. J. Matschull, “*Black Hole creation in 2 + 1 dimensions*”, *Class. Quantum Grav.* **16** (1999) 1069-1095 [arXiv:gr-qc/9809087].